International Journal of Medical Toxicology & Legal Medicine **Volume 27, No. 4, 2024**
e-ISSN: 0974-4614
p-ISSN: 0972-0448

A Hybrid CNN–ELM Approach for Accurate Brain Tumor Classification

Shashikant Agrawal[1], Supriya Tripathi[2]

[1]PhD. Research Scholar, Bhilai Institute of Technology, Durg, Chhattisgarh, India
[2] Professor, Bhilai Institute of Technology, Durg, Chhattisgarh, India

Received: 14.10.2024 Revised: 19.11.2024 Accepted: 13.12.2024

ABSTRACT
These days, brain tumors are among the most common health issues in many countries due to factors including career, genetics, and global warming. Gliomas are the most aggressive type of brain tumor, resulting in a high-grade life. A brain tumor can be saved if it is found and diagnosed early. Brain tumors are becoming one of the most common health problems in many countries throughout the world as a result of global warming, heredity, career, and other factors. Gliomas are the most aggressive type of brain tumor, and they have a long life. Early detection and diagnosis of a brain tumor can be life-saving. Magnetic Resonance Imaging (MRI) is a simple method for determining tumor location. However, the large number of data generated by MRI makes manual segmentation difficult to complete within a reasonable time frame, limiting the use of reliable quantitative metrics in clinical practice. An autonomous and dependable approach is required for effectively segmenting tumors. This paper provides a novel technique for brain tumor segmentation based on cascaded UNET architecture. Initially, the photos are downsized into 128 × 128 pixels to optimize computing time. Additionally, increased adaptive gamma correction is applied to the input photos to improve pixel quality. Training and validation are performed on selected slices including tumor areas. The suggested model has been validated using the BraTS 2020 dataset. The proposed work had an accuracy of 99.70%, 99.46% specificity, 96.14% sensitivity, and 98.25% precision. The proposed method performs better than earlier methods in terms of accuracy.

Keywords: Computer vision, MRI segmentation, and tumor area segmentation Sensitivity analysis and improved adaptive gamma correction UNET

INTRODUCTION

Computer-based systems are very important in biomedical engineering these days since they can do things that save lives, such Patient-Centric Monitoring, diagnosis, and surgery [11]. As the population ages, cancer is getting more common and is becoming a global health problem. Every year, some 12.7 million people receive a cancer diagnosis, and 7.6 million of them pass away from the disease. Every year, the number of cancer-related deaths rises.

It's hard to give a lot of information about most cancers because each one has several subtypes. The fifth most prevalent and deadliest kind of cancer is brain cancer.It follows esophageal, breast, uterine, and stomach cancer. According to the World Health Organization (WHO), there are over 120 distinct types of brain tumors. Brain tumors are defined by their location (primary or secondary), type of tissue, non-cancerous or cancerous (benign or malignant) cells, and other important factors [23]. Accurately calculating the relative volume of a brain tumor's subcomponents is essential for monitoring progression, radiation planning, outcome evaluation, and follow-up investigations. Manual tissue segmentation poses significant hurdles for human specialists due to the diverse manifestations of tumors and the necessity to analyze many images from varied MRI sequences to accurately classify the inspected tissue type. This tedious process is vulnerable to human error and is time-consuming, leading to considerable intra- and inter-rater variability [17]. Manual segmentation is labour-intensive and challenging in MRIs due to their multi-modality and large-volume 3D nature

Medical imaging is essential for the diagnosis, treatment planning, and follow-up of cancer patients. As part of treatment plans, the size and location of tumors are usually assessed. For radiation planning, clinicians must manually define target volumes, which is difficult and time-consuming. For visualizing brain tumors, magnetic resonance (MR) pictures are especially useful. Different MR sequences (T2, T2-FLAIR, T1, T1 + gadolinium) show different tumor subcomponents like the contrast-enhancing core, necrosis, and edema. Machine learning techniques have demonstrated remarkable performance in many image identification applications in recent years [21].

The key contributions of the proposed work are.

1. To suggest utilizing a customized CNN to segregate brain tumor regions from MRI images

2. To accurately perform and categorize the three stages of brain malignancies.
3. To segment brain tumor regions for a large dataset.

The literature review is organized in this study, just as it is in Section 2.The suggested parallel UNET architecture for brain tumor segmentation is described in depth in Section 3. Results and discussions are presented in Section 4 along with performance analysis and sample photos for the BRATS dataset. The task is concluded in Section 5.

LITERATURE SURVEY

Amin et al. (1) used MRI to classify different glioma grades non-invasively using a unique model that combines CNNs and Genetic Algorithms (GA). In contrast to conventional approaches that depend on trial and error or preset frameworks, GA allows for the investigation of many architectures when determining the CNN's design. By lowering the variance of the prediction mistakes, the ensemble algorithm—more especially, bagging—was used to increase the prediction accuracy even more. The results showed that the three Glioma grades could be classified with 90.9% accuracy.

An automatic detection method for MRI tumor grade classification was created by Kaur et al. (4). Using multilevel thresholding techniques based on edge and intensity magnitude, the Region of Interest (ROI) was defined. The PFree BAT optimization model adaptively defined the model parameters, including neighborhood size and fuzzy strength. When tested on the PD dataset, the adopted model had an accuracy of 97.45% and 98% with feature selection.

For the automatic classification and diagnosis of brain cancers, Mishra et al. (5) presented a unique method based on the Local Learning-Based Radial Basis Function Neural Network (LLRBFNN) method named MASCA (Modified ASCA) in conjunction with Particle Swarm Optimization (PSO). During the segmentation phase, the conventional FCM Fuzzy C-Means (FCM) algorithm-based method failed to eliminate noise from MR images. In order to smooth and lower noise in brain tumor MR images, the suggested model incorporated an improved, quick, and reliable FCM algorithm segmentation technique.

By merging sparse FCM (Fuzzy C-Means) and FCM clustering techniques, Sathish et al. (7) presented a clustering methodology known as Gaussian-based Hybrid Fuzzy C-Means (GHFC) and Fuzzy C-Means for segmentation. The Gaussian function was used in the segmentation process. Relevant features were collected from the brain tumor images following segmentation. In order to identify the training classes using a classifier, these extracted characteristics were subsequently utilized as training data for the "exponential cuckoo-based Rough Boost Neural Network (RBNN)." The experimental results of the suggested model demonstrated a low Mean Squared Error (MSE) and improved accuracy. The experiment was carried out using the BRATS and SIMBRATS databases.

Dolphin-SCA based deep CNN is a DL model that Sharan et al. (9) presented for the categorization of brain tumors. There was a pre-processing stage for the input MRI pictures. The segmentation process combined the fuzzy deformable fusion strategy with the Dolphin-SCA method. The features were extracted using statistical characteristics and Power LDP (Local Directional Pattern). These collected features were utilized to classify brain tumors using the DCNN and Dolphin-SCA algorithms. The selected model's experimental results demonstrated the highest level of accuracy and superior performance when compared to other conventional models for brain tumor classification.

A boundary-aware sampling method was presented by Lee et al. (12) with an emphasis on using features from picture patches situated at the ground-truth boundary area. This method was used to segment brain tumors and spinal cord gray matter in MRI images, as well as to segment the liver and lungs in CT and chest radiographs. The findings showed that this technique improved the segmentation performance of well-known deep learning (DL) models, including DeepLabV3+, U-Net, and U-Net++. The study also showed that contrastive embedding might be used to increase the robustness of domain shifts in segmentation tasks. These results demonstrate how the boundary-aware sampling approach can enhance DL-based segmentation tasks in a variety of medical imaging applications.

Geng et al. (13) investigated a pipeline approach for medical picture denoising and applied it as a generative adversarial network. The techniques such as U-Net, predictors,

DnCNN and SRDenseNet are examined. CT, PET, and MR imaging datasets have been used to confirm the model's efficacy. The results show that this system produced a best-in-class denoising procedure in terms of visual appeal and numerical measurements, and the technology has a great potential for generalization.

Ramya et al. (14) investigated how various k values—2, 4, 8, 16, 32, and 64—affect the predictive power of DL methods such as VGG-16, ResNet18, Inception V3, and VGG-19 for corn illnesses. According to the study, a k value of 32 produced better diagnostic recall and higher identification accuracy on samples for illnesses, rust, and leaf spot gray spot. The suggested approach used DL techniques to predict corn disease with an average diagnostic accuracy of 93%.

Proposed tumour region segmentation from MRI images

Brain tumor segmentation from MRI data can be efficiently performed using the U-Net architecture. The overall segmentation process is illustrated in Figure 1. It begins with reading and preprocessing the MRI slices. From the available image database, only the slices containing visible tumor regions are selected for further analysis. These selected slices are then divided into training and validation sets. The segmentation process makes use of the mask data provided in the dataset to accurately identify different tumor areas.

To simplify the model and reduce memory usage, each image is resized to 128 × 128 pixels, followed by enhanced adaptive gamma correction to improve image contrast. The U-Net model is then trained using separate masks corresponding to the enhancing

Tumor, non-enhancing tumor, and edema region.

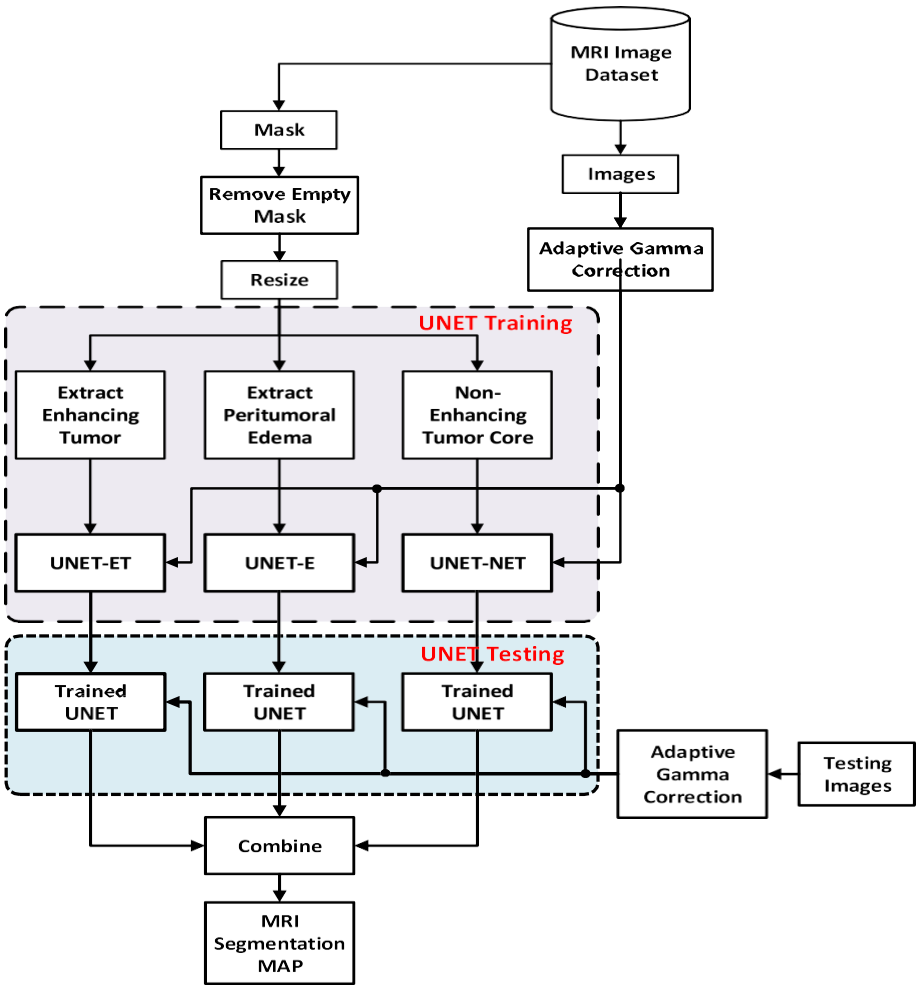

Fig 1. Brain Tumour segmentation using parallel UNET (Suggested)

Finally, the trained U-Net model is applied to the testing phase, where it performs segmentation on unseen MRI slices to validate the overall accuracy and performance of the network.

For segmenting and classifying the three types of tumor regions—edema, non-enhancing tumor, and enhancing tumor—three separate U-Net models are used. Each model is trained independently using its specific type of mask. Since these tumor regions differ in texture, brightness, and pixel intensity, each U-Net learns to recognize and classify them accurately.

During the training phase, labeled MRI images and their corresponding masks are taken from the dataset. Before training, all images are down sampled to a smaller size to speed up computation and reduce memory usage. However, care is taken to avoid excessive resizing, as it can reduce image quality and affect the model's accuracy.

In the testing phase, each MRI image is first enhanced and resized, then passed through the three trained U-Net models. Each network generates a segmentation map that highlights its respective tumor type. These maps are then merged to form a complete tumor segmentation. To improve accuracy and reduce variations among the models, a weighted voting method is used to combine the results, producing a more reliable final output.

The overall MRI image classification process starts by loading a training image and its corresponding mask from the dataset. After preprocessing and resizing the images to 128 × 128 pixels, they are grouped based on the mask labels into enhancing tumor, non-enhancing tumor, and edema categories. These images are then used to train the three U-Net models. Finally, both training and validation are carried out to evaluate the system's performance in classifying different tumor regions.

Block diagram

Improved adaptive gamma correction

A sophisticated image enhancement method called Improved Adaptive Gamma Correction (IAGC) is used in digital image processing to increase the visual quality of images by dynamically modifying the gamma correction parameter according to local image features.

Gamma correction is a nonlinear process used to make up for the nonlinear brightness response of displays and monitors. It guarantees that an image's perceived brightness and actual intensity match. Conventional gamma correction uses a single, set gamma value throughout the image, which could not work well for pictures with different contrast or uneven illumination.

For photos taken in situations with strong contrast, complex illumination, or uneven lighting, IAGC works very well [10,15]. To provide sharper and more aesthetically pleasing images, it is extensively utilized in computer graphics, photography, satellite imaging, and medical imaging.

The precision of image analysis and local gamma estimate are key factors in IAGC performance. Images taken in well-lit or typical lighting situations are already optically balanced, thus it might not make a big difference.

The ideal enhancement is achieved by experimentally determining a threshold value "t" that strikes a balance between computing efficiency and visual benefit [2,6,8,16]. The constant Tt, which is usually set at 128 for 8-bit images (half the maximum pixel intensity), represents

$$t = \frac{m_i - T_i}{T_i}$$

The estimated average brightness of natural images. In the course of analysis:

A picture is considered darkened if t is less than -Tt. An image is considered bright if t > -Tt. Images that fall into the typical brightness range are not eligible for AGC-based enhancement.

To enhance contrast in bright photos, an AGC technique based on negative images is used.

The Cumulative Distribution Function (CDF) truncation approach is used to restore brightness to photographs that have become faint.

Combining these two techniques, the suggested method successfully improves both bright and dark photographs, adjusting to their particular lighting conditions and generating visually consistent, excellent results [18,19].

The block diagram describing the increased adaptive gamma correction procedure is shown in Figure 2. Digital image processing depends on the sort of image being classified. When dealing with a bright image, the procedure entails applying adaptive gamma correction after a negative image modification. Based on the picture, the procedure is broken down as follows: The block diagram illustrates a method for improving pictures according to their brightness. An input image is first used, and it is then classified according to its brightness level. categorized as either muted image processing or bright image processing. This classification takes place at the "Type" decision point.

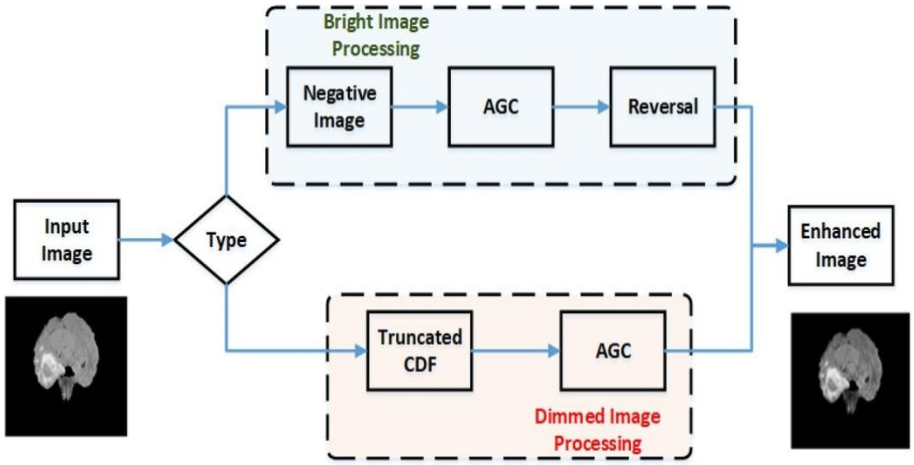

Fig.2 Block diagram for Improved Adaptive Gamma Correction

Convolutional neural network UNET

U-Net is a convolutional neural network that was first developed for the medical field's biological picture segmentation needs. The main idea is to add successive layers to a typical contractual network to improve it. These additional layers improve performance by substituting up sampling operators for pooling operations. As a result, this layering arrangement helps to improve the output's resolution. The network's precise segmentation capabilities are then enhanced by a subsequent convolutional layer that can learn from the data of the previous layer and produce a more refined output. The contracting route mimics the structure of a traditional convolutional network by applying convolutions repeatedly, each followed by an activation of a rectified linear unit (ReLU) and a max-pooling operation [3,20]. In order to accomplish spatial contraction and simultaneously enhance feature information, this sequence is repeated. The expansive route, on the other hand, concentrates on merging high-resolution data with feature and spatial information from the contracting path. This is accomplished by a sequence of concatenations and up-convolutions that successfully incorporate the learned data. Combining these two paths creates the unique U-shaped network architecture, which allows the network to efficiently capture and fine-tune features at various scales while preserving spatial information.

(1) $$Loss_b^x = -\sum_{i=1}^{k+m} \sum_{x,y} w_{x,y}^i \ log\,[p_{i,(x,y)}^l(\theta)]$$

Where $p_{i,(x,y)}^l$ is the arrangement Notch is the presumed weight of the pixel and is agreed upon by the organization to be the ground truth for pixel (x,y) of the ith image of the consignment. The loads are used to reduce the effect of class unevenness because cancer pixels only make up a small portion of the image.

Training: - Caffe's stochastic gradient descent is used with segmentation maps and input images during training. Unpadded convolutions maintain consistent borders between input and output. Large input tiles with smaller batch sizes optimize GPU memory and computation. A high momentum of 0.99 ensures effective sample updates. The final feature map passes through SoftMax, combined with cross-entropy loss to compute the energy function. This approach enhances network segmentation and overall performance. The soft-max is defined as

pk(x)=exp(ak(x))/pk(x)=exp()k=1exp(ak(x))

(2)

whereak(x)denotestheactivationinfeaturechannelkatthepixelpositionx∈Ωwith Ω⊂Z2.Kisthenumberofclasses,andpk(x)istheapproximatedmaximumfunction.I.e.pk(x)≈1forthekthathasthemaximumactivationak(x)andpk(x)≈0forallotherk.Thecross-entropy then penalizes at each position the deviation of p(x)(x) from 1 using

$$E = \sum_{x\epsilon\Omega} \omega(x) \log\,(pl_{(x)}(x)) \quad (3)$$

where:Ω→{1...,K}is the true label of each pixel, and w:Ω→R is a weight map that is Introduced to give some pixels more importance in training. It is necessary to pre-compute the weight map for each ground truth segmentation to compensate for the different frequency of pixels from a specific class in the training dataset and force the network to learn the small separation borders between touching cells are introduced. The separation boundary is calculated by performing morphological operations on the data. The weight map is then calculated in the following way:

(4) $$\omega(x) = \omega_c(x) + \omega_0 . \exp\,(-\frac{(d_1(x)+d_2(x))^2}{2\sigma^2})$$

where c: Ω → R is the weight map to balance the class frequencies, d_1: Ω → R denotes the distance to the border of the nearest cell, and d_2: Ω → R is the distance to the border of the second nearest cell. In the experiments, set 0 = 10 and σ ≈ 5 pixels.

Figure 3 shows the UNET Architecture used for MRI segmentation. Here, the input image is resized to 128 × 128, which is the input layer size of UNET. UNET architecture used for MRI image segmentation consists of 9 Layers, as shown in Fig. 3. The final layer performs the decision-making process. The sigmoid activation function is used in this layer to perform the decision-making process.

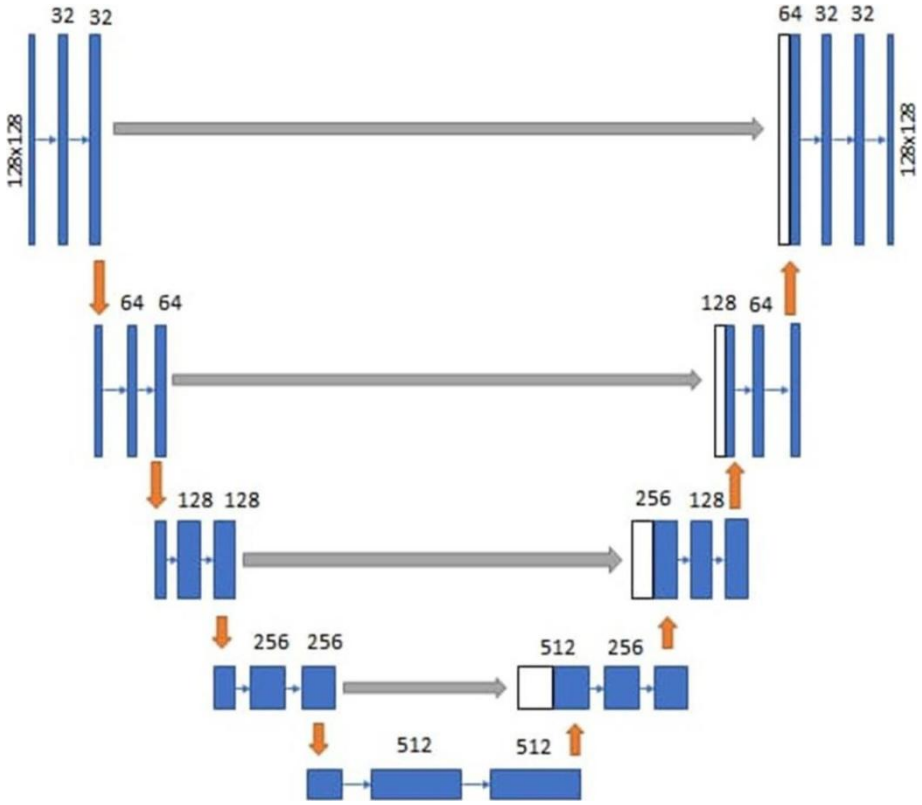

Fig.3 UNET Architecture used for MRI segmentation

RESULT AND DISCUSSION

The proposed MRI segmentation is implemented in Python. The BraTS 2020 dataset, available on Kaggle, is accessed and processed using Python commands. Selected image slices are utilized for training and validation. The UNET architecture is developed using TensorFlow and scikit-learn libraries. Detailed information about the BraTS 2020 dataset is provided in the following section.

Dataset

The proposed network's performance is evaluated using the BraTS 2020 dataset. It includes 369 training, 125 validations, and 169 test multimodal MRI scans. Each scan contains T1, T1ce, T2, and FLAIR sequences. All MR images have a resolution of 240 × 240 × 155. Experts labeled three tumor regions: necrotic and non-enhancing core (NET), peritumoral edema (ED), and enhancing tumor (ET). Training annotations are publicly available for evaluation, while validation and test labels remain confidential.

A collection of sample photos taken from the BraTS 2020 dataset is shown in Figure 4.

Pictures from the BraTS 2020 dataset

(https://www.kaggle.com/datasets/awsaf49/brats2020-training-data) are used as input pictures in Figure 4 (a). However, a mask picture taken from the same database is shown in Figure 4 (b). Different areas within the MRI images are delineated by the mask picture. The MRI image's background is represented by the black area inside the mask. The non-enhancing tumor area is indicated by the white area. In the meantime, the central part of the mask shows the edema seen in the brain MRI, while the gray area represents the augmenting tumor site.

The result obtained by applying the improved adaptive gamma correction method is shown in Figure 5. The input image under examination is represented by the displayed image in Figure 5(a). The output obtained following the application of the enhanced adaptive gamma correction technique is shown in Figure 5(b). The comparison clearly shows that the application of increased adaptive gamma correction results in improvements, which are especially noticeable in the textural area of the tumor portion, as shown in Figure 5(b). This improvement highlights the efficiency of the used technique in enhancing image quality and information by helping to produce a better and more distinct depiction of the unique features and traits present within the tumor area.

Performance metrics

Accuracy

The percentage of accurate predictions per total number of forecasts is a measure of a system's accuracy. Interestingly, the accuracy of the suggested method is noticeably higher than that of earlier techniques.

(5)
$$\text{Accuracy} = \frac{Tp+Tn}{(TP+TN+FP+FN)} \times 100\%$$

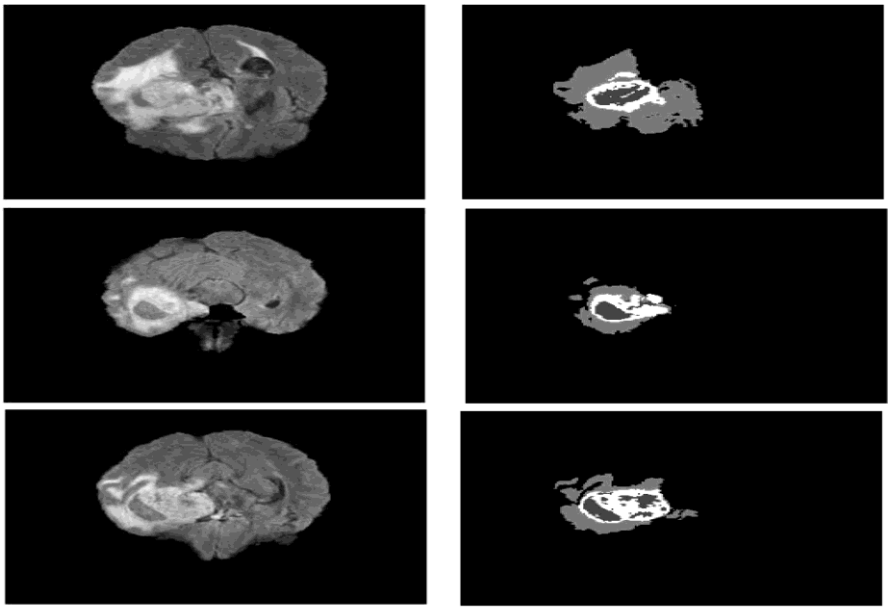

Fig 4. Sample Images from the dataset a. Input Image, b. Mask

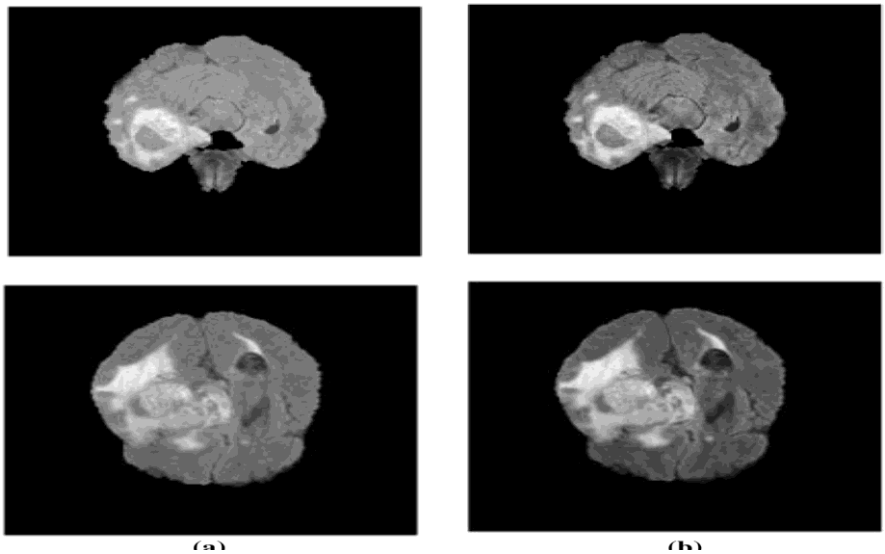

Fig. 5 Improved image using Enhanced Adaptive Gamma Correction technique: (a) Input image, (b) Enhanced adaptive gamma-corrected image

Sensitivity

A system's accuracy is calculated by dividing the number of correct predictions by the total number of forecasts. Importantly, the proposed strategy outperforms previous techniques in terms of accuracy.

(6)
$$\text{sensitivity} = \frac{\text{Tp}}{\text{Tp+Fn}} \times 100$$

where Tp which are positive instances correctly classified as positive, False Positives (FP), which are negative instances incorrectly classified as positive, True Negatives (TN), which are negative instances correctly

classified as negatives, and False Negatives (FN), which are positive instances incorrectly classified as negatives.

Specificity

This word refers to the ratio of true negative samples to total negative samples in the data set. It should be elevated. The calculation of the specificity is

(7) $$specificity = \frac{Tn}{Tp+Fn} \times 100$$

Precision

Precision is defined as the percentage of positives that were accurately recognized as positive. The formula for calculating precision is shown below.

(8) $$precision = \frac{Tp}{Tp+Fp} \times 100$$

F1 Score

One statistic that considers both recall and precision in a classification system is the F1 Score. It is computed as the average of precision and recall, or the harmonic mean. In situations when the system must balance recall and precision, the F1 Score is especially helpful. This formula provides comprehensive assessment of the classification performance by capturing combined effects of precision and recall.

(9) $$\text{F1Score} = \frac{\text{Tp}}{\text{Tp}+0.5\,(\text{Fp}+\text{Fn})} \times 100$$

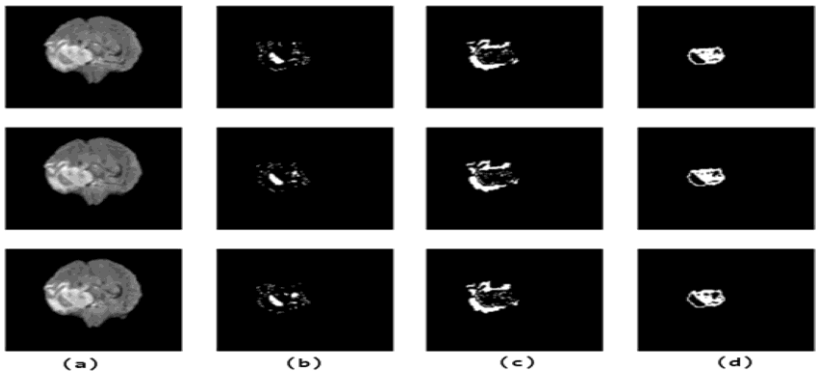

Fig. 6 (a) Input images from the dataset, (b) Segmented Enhancing Tumour Region, (c) Non-enhancing Tumour, (d) Edema image

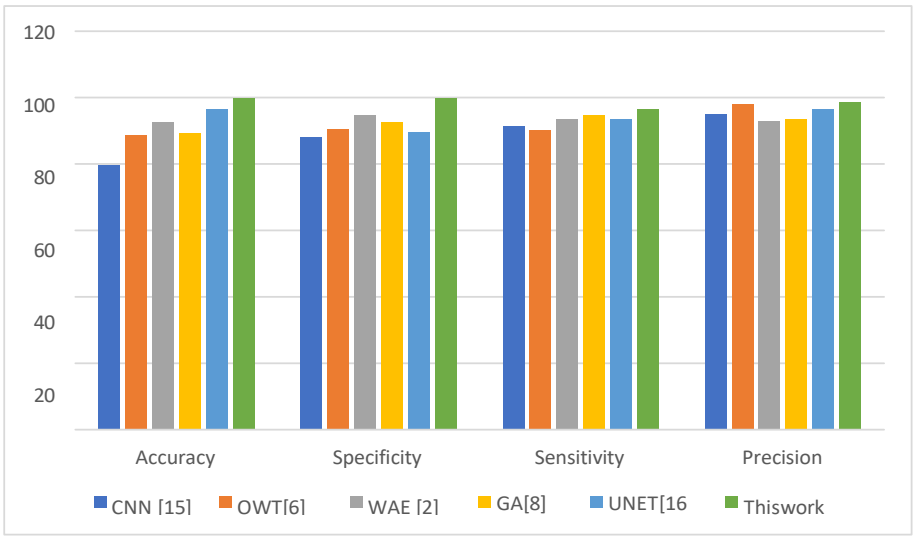

Fig.7 Comparison of the Proposed Method with Existing Approaches

DISCUSSION

The input photos and the segmentation maps that go with them are displayed in Figure 6. Three MRI slices from subject 1 are shown in Figure 6a.

Fig. 8 Validation and training loss concerning the number of iterations

Fig. 9 Validation and training accuracy concerning the number of iterations

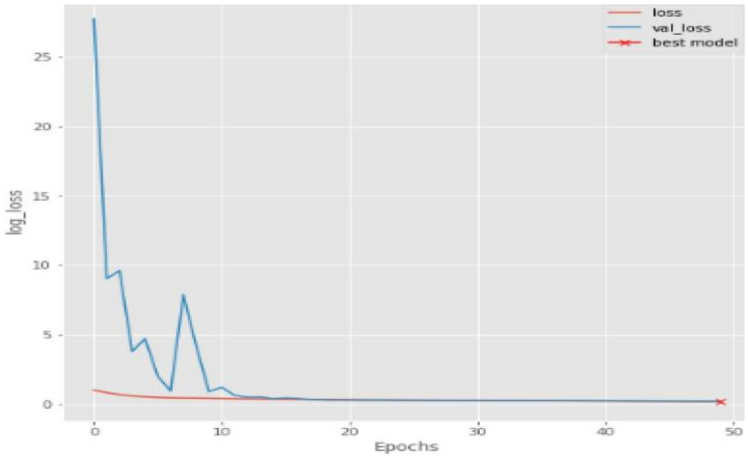

Fig. 10 Training and validation loss for non-enhancing tumour UNET training process

The segmentation map produced by the UNET trained to enhance tumor areas is shown in Figure 6b. The map from the UNET trained for non-enhancing tumor locations is displayed in Figure 6c, while the map for the edema region is shown in Figure 6d. The suggested strategy is contrasted with earlier strategies in Figure 7. Training and validation loss over several epochs are shown in Figure 8. For the non-enhancing tumor UNET model, Figure 10 illustrates training and validation losses while Figure 9 shows validation and training accuracy vs iteration count. Figure 11 displays the training and validation loss for increasing the tumor UNET training process. Figure 12 depicts the Training and validation loss for edema UNET training procedure. The performance of the suggested iteration-based approach is shown in Table 1. Accuracy for improving tumors

rose from 89.56% at 50 iterations to 98.58% at 100 iterations. Accuracy increased from 90.25% to 97.60% for edema tumors. Accuracy increased from 90.63% to 98.62% for non-enhancing tumors. Training and validation results are displayed in Table 2. Accuracy was 95.2%, validation accuracy was 95.25%, and validation loss was 0.5109 after 25 iterations. Accuracy was 96.8%, validation accuracy was 96.05%, and validation loss was 0.4419 after 30 iterations. Validation accuracy achieved 98.26%, validation loss dropped to 0.1521, and accuracy increased to 98.5% after 50 iterations.

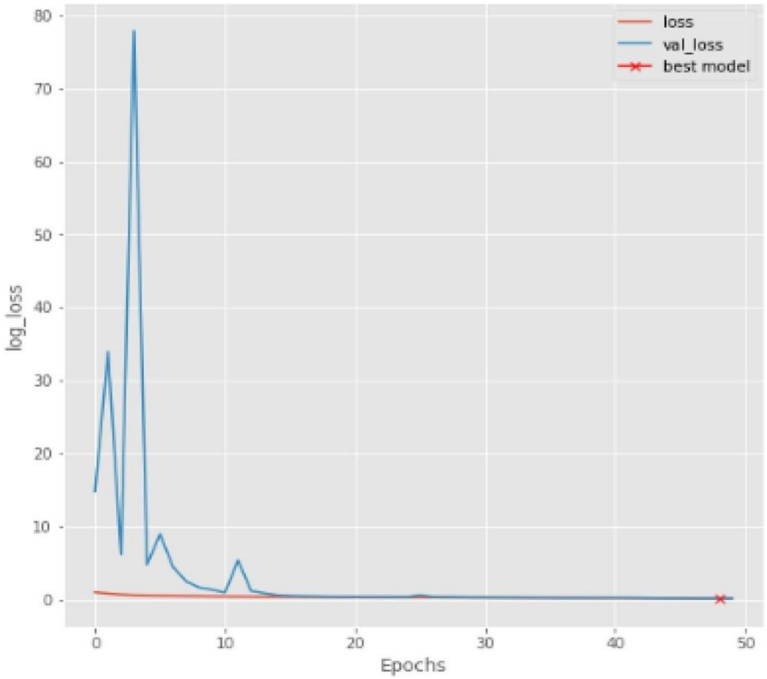

Fig. 11 Training and validation loss for enhancing tumour UNET training process

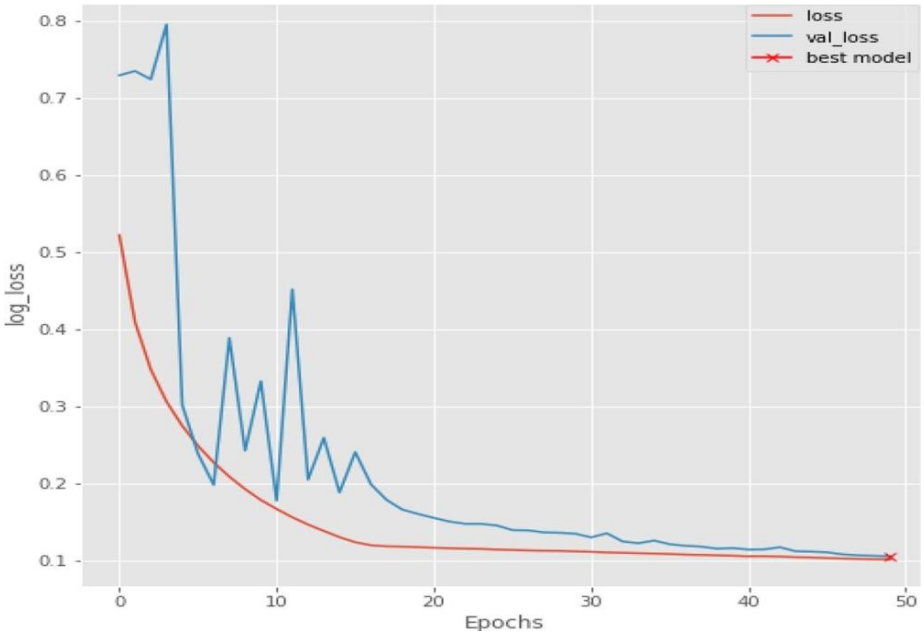

Fig.12 Training and validation loss for edema UNET training process

The performance of the suggested approach based on various training-to-testing ratios is displayed in Table 3. The model attains 99.71% accuracy, 98.99% specificity, and 98.46% sensitivity using 75% training and 25% testing pictures. Reversing the ratio (75% testing and 25% training) results in lower performance. The suggested methodology is contrasted with conventional methods in Table 4. 78.51% accuracy, 87.20% specificity, 90.48% sensitivity, and 93.48% precision are attained with the CNN [15] approach. 87.51% accuracy, 90.50% specificity, 89.15% sensitivity, and 96.81% precision are achieved using the OWT [6] approach. 91.42% accuracy, 93.80% specificity, 92.41% sensitivity, and 91.80% precision are offered by the

WAE [2] method. The accuracy of the GA [8] method is 88.34%., 90.41%specificity,92.81% sensitivity,and 92.45% precision. The UNET [16] approach yields 95.40% accuracy,

Table 1: Testing performance of proposed method based on iteration

Iteration	Metrics	50	60	70	80	90	100
EnhancingTumour	Accuracy	89.56	92.80	92.81	97.39	97.88	98.58
	Sensitivity	98.35	95.80	85.45	97.10	97.18	97.90
	Specificity	97.40	96.19	92.23	97.74	97.80	97.95
Edema	Accuracy	90.25	90.67	91.10	95.21	96.89	97.60
	Sensitivity	90.52	91.16	91.48	95.27	95.92	98.25
	Specificity	90.23	91.54	91.65	95.83	95.81	98.10
non-EnhancingTumourCore	Accuracy	90.63	92.82	92.82	97.42	97.91	98.62
	Sensitivity	90.67	95.84	85.49	97.13	97.23	97.93
	Specificity	90.85	96.18	92.25	97.76	97.81	97.99

Table 2: Training and validation performance

No of iteration	Training loss	Training Accuracy	Validation loss	Validation Accuracy
25	0.5212	95.2	0.5109	95.246
30	0.4628	96.8	0.4419	96.047
35	0.4125	96.3	0.3909	96.555
40	0.3620	97.4	0.3318	97.315
45	0.2514	98.2	0.2346	98.098
50	0.1474	98.5	0.1521	98.259

Table 3: Performance of proposed method based on the ratio of testing and training

Testing	Training	Acc	Spe	Sen	F1-Score
75	25	72.89	66.94	70.43	81.658
50	50	86.43	82.61	88.31	90.125
25	75	99.71	98.99	98.46	98.92

88.41% specificity, 92.42% sensitivity, and 95.42% precision. With 99.70% accuracy, 99.46% specificity, 96.14% sensitivity, and 98.25% precision, this work also performs well in comparison to previous research.
The UNET requirements utilized in the suggested work to create the segmentation map are shown in Table 5. For better speed, the UNET's input size is 128 x 128. Additionally, 128 x 128 is the output size. The segmentation process is carried out by the UNET's nine tiers. The weight optimization procedure is carried out using the Adam training approach. The validation procedure is carried out using a 75:25 training testing ratio.
The planned study's confusion matrix is shown in Table 6. Pixel-level categorization is used to build the matrix. It is produced by comparing ground truth photographs with anticipated outcomes. Non-Enhancing Tumor, Enhancing Tumor, and Edema are the three classifications that are employed. Table 6 illustrates that 15,423 pixels are accurately diagnosed as non-enhancing tumors, but 123 and 102 pixels are recognized as enhancing tumors and edema, respectively. As seen in Table 6, incorrect classifications for additional classes are also noted.

Table 4: Performance of proposed method concerning conventional techniques

Methods	Accuracy	Specificity	Sensitivity	Precision
CNN[15]	78.51	87.20	90.48	93.84
OWT[6]	87.51	90.50	89.15	96.81
WAE[2]	91.42	93.80	92.41	91.80
GA[8]	88.34	90.41	92.81	92.45
UNET[16]	95.40	88.41	92.42	95.42
Thiswork	99.70	99.46	96.14	98.25

Table 5: UNET specifications

1	InputSize	128×128
2	OutputSize	128×128
3	OutputLabels	4
4	NumberofFilters	16
5	MinimumLearningRate	0.00001
6	BatchSize	32
7	MinimumEpoch	50
8	LossFunction	BinaryCrossEntropy
9	TrainingAlgorithm	Adam
10	Dropout	0.05
11	TrainingTestingRatio	75:25
12	NumberofLayers	9

Table 6: Confusion matrix

	Non-Enhancing Tumour	Enhancing Tumour	Edema
Non-Enhancing Tumour	15423	251	12
Enhancing Tumour	123	15236	2
Edema	102	120	5326

CONCLUSION

An enhanced technique for brain tumor segmentation is presented in this paper. Non-enhancing, enhancing, and edema areas are categorized using three UNET models. First-stage contrast is improved with an improved adaptive gamma correction. The BraTS 2020 dataset is utilized for training and assessment using optimum settings. To improve accuracy, mask pictures are divided into three zones for independent UNET training. The algorithm's performance is assessed using sensitivity analysis with different training and testing ratios. 99.70% accuracy, 99.46% specificity, 96.14% sensitivity, and 98.25% precision are attained by the suggested approach. UNET weight optimization may be used to further increase class-wise classification accuracy.

REFERENCES

1. Amin Kabir Anaraki, Moosa Ayati & Foad Kazemi 2018, „Magnetic resonance imaging-based brain tumor grades classification and grading via convolutional neural networks and genetic algorithms", Biocybernetics and Biomedical Engineering, vol. 39, no. 1, pp. 63-74.
2. Abd El Kader I, Xu G, Shuai Z, Saminu S, Javaid I, Ahmad IS, Kamhi S (2021) Brain tumour detec-tion and classification on MRimages by a deep wavelet auto-encoder model.Diagnostics11(9):1589
3. Aghalari M, Aghagolzadeh A, Ezoji M (2021) Brain tumour image segmentation via asymmetric/sym-metricUNetbasedontwo-pathway-residualblocks.BiomedSignalProcessControl69:102841
4. Kaur, T, Saini, BS & Gupta, S 2019, „An adaptive fuzzy K-nearest neighbor approach for MR brain tumor image classification using parameter free bat optimization algorithm", Multimedia Tools Appl, vol. 78, pp. 21853–21890, https://doi.org/10.1007/s11042-019-7498-3.
5. Mishra, S, Sahu, P & Senapati, MR 2019, „MASCA–PSO based LLRBFNN model and improved fast and robust FCM algorithm for detection and classification of brain tumor from MR image", Evol. Intel., vol. 12, pp. 647–663, https://doi.org/10.1007/s12065-019-00266-x.
6. Arif M, Ajesh F, Shamsudheen S, Geman O, Izdrui D, Vicoveanu D (2022) Brain tumour detectionand classification by MRI using biologically inspired orthogonal wavelet transform and deep learningtechniques. J Healthc Eng 2022:1–18
7. Sathish, P & Elango, NM 2020, „Gaussian hybrid fuzzy clustering and radial basis neural network for automatic brain tumor classification in MRI images", Evol. Intel, https://doi.org/10.1007/s12065-020-00433-5.
8. Aswathy SU, Glan Devadhas G,Kumar SS(2019)Braintumour detection and segmentation using a wrapper-based genetic algorithm for the optimized feature set. ClustComput 22(6):13369–13380
9. Sharan Kumar & Dattatreya P Mankame 2020, „Optimization driven Deep Convolution Neural Network for brain tumor classification", Biocybernetics and Biomedical Engineering, vol. 40, no. 3, pp. 1190-1204.
10. Cao G, Huang L, Tian H, Huang X, Wang Y, Zhi R (2018) Contrast enhancement of brightness-dis-tortedimagesbyimprovedadaptivegammacorrection.ComputElectrEng66:569–582
11. ChakrabortyC,KishorA(2022)Real-timecloud-basedpatient-centricmonitoringusingcomputa-tional health systems. IEEE transactions on computational social systems 9(6):1613–1623

12. Lee, H.H.; Novikov, D.S.; Fieremans, E. Removal of partial Fourier-induced Gibbs (RPG) ringing artifacts in MRI. Magn. Reson. Med. 2021.
13. Huang C, Wan M (2022) Automated segmentation of brain tumor based on improved U-Net with residual units. Multimedia Tools Appl 81(9):12543–12566.
14. Ramya Manaswi, V., &Sankarababu, B. (2022). A Flexible Accession on Brain Tumor Detection and Classification Using VGG16 Model. In Smart Intelligent Computing and Applications, Volume 1 (pp. 225-238). Springer, Singapore.
15. Gull S, Akbar S, Khan HU (2021) Automated detection of brain tumour through magnetic resonance images using convolutional neural network. BioMed Res Int 2021:1–4
16. Huang C, Wan M (2022) Automated segmentation of brain tumour based on improved U-Net with residual units. Multimed Tools Appl 81(9):12543–12566
17. Kamnitsas K, Ferrante E, Parisot S, Ledig C, Nori A. V, Criminisi A … Glocker B (2016) Deep- Medic for brain tumour segmentation. In: International workshop on brainlesion: glioma, multiple sclerosis, stroke and traumatic brain injuries. Springer, Cham, pp 138–149
18. Latif U, Shahid AR, Raza B, Ziauddin S, Khan MA (2021) An end-to-end brain tumour segmenta- tion system using multi-inception-UNET. Int J Imaging Syst Technol 31(4):1803–1816
19. Pravitasari AA, Iriawan N, Almuhayar M, Azmi T, Irhamah I, Fithriasari K, Purnami SW, Ferriastuti W (2020) UNet-VGG16 with transfer learning for MRI-based brain tumour seg- mentation. TELKOMNIKA (Telecommunication Computing Electronics and Control) 18(3):1310–1318
20. Wang G, Lu H, Wang Y, Zhao C (2022) A novel brain tumour segmentation method based on im-proved spatial attention mechanism and multi-path deep neural network. J Phys Conf Ser 2203(1):012057. IOP Publishing
21. Zhou C, Chen S, Ding C, Tao D (2018) Learning contextual and attentive information for brain tumour segmentation. In: International MICCAI brainlesion workshop. Springer, Cham, pp 497–507.